Research Square

Preprints are preliminary reports that have not undergone peer review.
They should not be considered conclusive, used to inform clinical practice,
or referenced by the media as validated information.

Perineuronal nets enwrap dysmorphic neurons and parvalbumin interneurons at the seizure onset zone of focal cortical dysplasia type IIb

Sophia Auer

sophia.auer@fau.de

Friedrich-Alexander-Universität Erlangen-Nürnberg

Johanna Samusch

Friedrich-Alexander-Universität Erlangen-Nürnberg

Stefan Rampp

Universitätsklinikum Erlangen

Vadym Gnatkovsky

University Hospital Bonn

Ahmed Gaballa

Krankenhaus Mara

Christian Günther Bien

Krankenhaus Mara

Till Hartlieb

Schön Klinik Vogtareuth

Lucas Hoffmann

Universitätsklinikum Erlangen

Martin Schicht

Friedrich-Alexander-Universität Erlangen-Nürnberg

Friedrich Paulsen

Friedrich-Alexander-Universität Erlangen-Nürnberg

Ingmar Blümcke

Universitätsklinikum Erlangen

Article

Keywords: Focal cortical dysplasia, Perineuronal net, Parvalbumin, Dysmorphic neuron, Extracellular matrix, Epilepsy surgery

Posted Date: November 27th, 2026

DOI: https://doi.org/10.21203/rs.3.rs-11812088/v1

License: This work is licensed under a Creative Commons Attribution 4.0 International License.
Read Full License

Additional Declarations: Competing interest reported. V.G. has advisory agreements with Brainlab AG and with Persyst Development Corporation, whose software was used for the SEEG analysis in this study; neither company had any role in the study design, data analysis, interpretation of the findings or the decision to publish. The other authors have no relevant financial or non-financial interests to disclose.

Perineuronal nets enwrap dysmorphic neurons and parvalbumin interneurons at the seizure onset zone of focal cortical dysplasia type IIb

Sophia Auer[1], Johanna Samusch[1], Stefan Rampp[2,3,4], Vadym Gnatkovsky[5], Ahmed Gaballa[6], Christian G. Bien[6], Till Hartlieb[7,8], Lucas Hoffmann[9], Martin Schicht[1], Friedrich Paulsen[1,†], Ingmar Blümcke[9,†]

[1]Institute of Functional and Clinical Anatomy, Friedrich-Alexander-Universität Erlangen-Nürnberg (FAU), Universitätsstraße 19, 91054 Erlangen, Germany
[2]Department of Neuroradiology, Universitätsklinikum Erlangen and FAU, Erlangen, Germany; member of the European Reference Network (ERN) EpiCARE
[3]Department of Neurosurgery, Universitätsklinikum Erlangen and FAU, Erlangen, Germany; member of ERN EpiCARE
[4]Department of Neurosurgery, University Hospital Halle (Saale), Halle (Saale), Germany
[5]Department of Epileptology, Universitätsklinikum Bonn, Bonn, Germany; member of ERN EpiCARE
[6]Department of Epileptology, Krankenhaus Mara, Bethel Epilepsy Center, Medical School, Bielefeld University, Bielefeld, Germany
[7]Center for Pediatric Neurology, Neurorehabilitation, and Epileptology, Schön Klinik Vogtareuth, Vogtareuth, Germany
[8]Research Institute for Rehabilitation, Transition, and Palliation, Paracelsus Medical University, Salzburg, Austria
[9]Department of Neuropathology, Universitätsklinikum Erlangen and FAU, Erlangen, Germany; member of ERN EpiCARE

[†]Friedrich Paulsen and Ingmar Blümcke contributed equally and share senior authorship.

Corresponding author: Sophia Auer, Institute of Functional and Clinical Anatomy, Friedrich-Alexander-Universität Erlangen-Nürnberg (FAU), Universitätsstraße 19, 91054 Erlangen, Germany. E-mail: sophia.auer@fau.de; Phone: +49 9131 85-26734; Fax: +49 9131 85-22862

Acknowledgements: We thank Elke Kretschmar and Andrea Eichhorn for technical support with electron microscopy, and Jörg Pekarsky (Institute of Functional and Clinical Anatomy, FAU) for the illustration in Fig. 7. This article is part of the doctoral thesis of S.A., performed in fulfilment of the requirements for the degree 'Dr. rer. nat.' at the Faculty of Sciences of the Friedrich-Alexander-Universität Erlangen-Nürnberg (FAU). This work was supported by the Deutsche Forschungsgemeinschaft (German Research Foundation), project 460333672, CRC1540 Exploring Brain Mechanics.

Abstract

Focal cortical dysplasia ILAE type IIb (FCDIIb) is an important cause of drug-resistant focal epilepsy in children, yet the cellular architecture that renders the lesion epileptogenic remains incompletely understood. We studied perineuronal nets (PNNs), parvalbumin (PV)-positive interneurons and dysmorphic neurons (DN) in surgical specimens from 20 patients with FCDIIb and in frontal cortex from 11 individuals without epilepsy using aggrecan immunohistochemistry and multiplex immunofluorescence. Perisomatic vesicular GABA transporter (VGAT)-positive puncta were quantified in 11 tissue blocks from eight patients and transmission electron microscopy was performed on tissue from one additional patient with FCDIIb. PNN density was increased in lesional compared with perilesional and control cortex and rose more steeply with age in FCDIIb. The densities of PV- and GAD-positive interneurons were preserved, but these cells were more frequently enwrapped by PNNs. In addition, PNNs were recruited to a subset of DN immunoreactive for non-phosphorylated neurofilament H and phospho-S6, which accounted for about one quarter of all PNN-bearing cells in lesional cortex, whereas balloon cells never carried PNNs. Net-enwrapped DN received denser perisomatic VGAT-positive innervation than DN without PNNs, partly from synaptotagmin-2-positive terminals, and electron microscopy confirmed symmetric axosomatic synapses on DN. In ten patients investigated with stereo-EEG, co-registration of 16 electrode contacts with MRI and histological sections showed higher PNN-enwrapped DN density around contacts generating the ictal-onset fast-activity pattern known as the Chirp than around non-Chirp contacts (linear mixed-effects model, $P < 0.001$). Neither total DN density nor PNN-enwrapped PV interneuron density differed significantly between contact classes. These findings identify a lesion-specific reorganization of the perineuronal extracellular matrix that links fast-spiking interneurons and dysmorphic neurons within a spatially restricted microdomain and suggest that this microdomain is a structural substrate of seizure onset in FCDIIb.

Keywords: Focal cortical dysplasia · Perineuronal net · Parvalbumin · Dysmorphic neuron · Extracellular matrix · Epilepsy surgery

Introduction

Focal cortical dysplasia ILAE type II (FCDII) is the most common histopathological finding in children undergoing epilepsy surgery for drug-resistant focal seizures [15, 51]. Its hallmarks, dysmorphic neurons (DN) and, in type IIb (FCDIIb), balloon cells, are well defined, and somatic variants in genes of the mTOR pathway explain the abnormal growth and differentiation of these cells [12, 16, 62]. Seizures arise within or immediately adjacent to the dysplastic cortex, and DN show altered intrinsic and synaptic properties that make them candidate generators of epileptic activity [25, 72, 84]. Yet the lesion is present continuously, whereas seizures occur only intermittently and, in FCDII, preferentially from non-rapid eye movement (NREM) sleep [34]. Which cellular arrangement within the lesion converts a fixed malformation into a site of seizure onset remains unresolved.

GABAergic interneurons constitute about one fifth to one quarter of all neurons in the primate neocortex [45] and can be subdivided by their content of the calcium-binding proteins (CaBPs) parvalbumin (PV), calbindin-D28k and calretinin, which serve as selective markers of nerve cells and label largely non-overlapping populations with distinct morphology, laminar distribution and synaptic targets [2, 23, 26, 29, 47]. PV-positive (PV^+) basket and chandelier cells are fast-spiking and provide perisomatic and axo-axonic inhibition to pyramidal cells [22, 48, 49]. Studies of human FCD have reported reduced densities of CaBP-immunoreactive interneurons [38, 54, 77, 88], abnormally large PV^+ neurons [37], but also preserved PV^+ interneurons with dense perisomatic baskets around dysmorphic cells [1, 60, 77, 80]. How inhibitory circuits are organized within FCDIIb therefore remains controversial.

PV^+ interneurons are typically enwrapped by perineuronal nets (PNNs), lattice-like condensations of the extracellular matrix composed of hyaluronan, chondroitin sulfate proteoglycans such as aggrecan, link proteins and tenascin-R [17, 24, 36]. PNNs cluster with Kv3.1b potassium channels, support the fast-spiking phenotype, restrict synaptic plasticity and cooperate with perisynaptic astrocytic processes [8, 21, 35, 44, 64, 81]. PNN alterations have been reported in experimental epilepsy, hippocampal sclerosis and the epileptic human hippocampus [52, 59, 67, 75], and PNNs were recently observed around DN in human epileptic tissue [28]. A systematic quantitative analysis of which cells carry PNNs in FCDIIb, and of how PNN coverage relates to the inhibitory innervation of DN, has not been performed.

Here, we quantified PNNs, PV^+ and GAD^+ interneurons and DN in lesional, perilesional and non-epileptic control cortex, characterized the perisomatic inhibitory innervation of DN by

immunofluorescence and electron microscopy, and, in a subgroup of patients investigated with stereo-EEG (SEEG), related these features to the sites generating the ictal-onset low-voltage fast-activity pattern known as the Chirp [27, 31, 41, 42, 53], using a previously established co-registration of SEEG contacts, MRI and histological sections [66].

Materials and methods

Patients and tissue samples

Surgically resected frontal lobe tissue was obtained from 22 patients with histopathologically confirmed FCDIIb who underwent epilepsy surgery between 2005 and 2025 at the Universitätsklinikum Erlangen, the Schoen Clinic Vogtareuth and the Bethel Epilepsy Center, Bielefeld, Germany (Table 1). Histopathological evaluation followed the ILAE consensus classification and recommendations [11, 16, 62]. All specimens were formalin-fixed and paraffin-embedded (FFPE). Twenty patients (P1-P20) contributed specimens to the quantitative immunohistochemical analysis. Nine of these patients (P12-P20) and one additional patient (P21) underwent SEEG before surgery; because some contributed more than one tissue block, 16 tissue slabs with histologically identifiable electrode trajectories were available for spatial analysis. A subset of 11 tissue blocks from eight patients was included in the analysis of perisomatic inhibitory terminals, and one additional FCDIIb specimen (P22) was fixed for transmission electron microscopy (TEM). *Postmortem* frontal lobe tissue obtained at autopsy from 11 individuals without a history of epilepsy or seizures served as control (Table 1); neuropathological review excluded relevant lesions such as tumor, neurodegeneration or neuroinflammation.

Definition of lesional and perilesional cortex

On aggrecan-immunostained whole sections, lesional cortex was defined by the presence of DN, balloon cells and dyslamination, and perilesional cortex as neocortex of the same specimen in which these features were absent or only sparse (Fig. 1d). Perilesional cortex was identifiable in nine specimens. Annotations were drawn by an experienced neuropathologist (I.B.) on the corresponding haematoxylin–eosin and SMI32-stained sections.

Immunohistochemistry and immunofluorescence

FFPE blocks were sectioned at 3 µm (Microm, Germany) and mounted on SuperFrost Plus slides (Epredia, USA). Immunohistochemistry was performed on a Ventana BenchMark

ULTRA (Roche Diagnostics). PNNs were visualized with anti-aggrecan antibodies (ACAN; 13880-1-AP, RRID: AB_2722780, rabbit IgG, 1:400; Proteintech, USA) and the OptiView DAB IHC Detection Kit, with haematoxylin counterstain. For immunofluorescence, slides were deparaffinized and subjected to microwave antigen retrieval in citrate buffer (pH 6; 3 min at 850 W, 2 × 10 min at 250 W, cooling to 50 °C on ice, 3 min at 850 W, 15 min on ice), rinsed in PBS (Biochrom, Germany) and blocked for 1 h at room temperature in 3% fetal bovine serum (Gibco, Thermo Fisher Scientific, USA), 1% goat serum (Agilent Dako, USA) and 0.1% Triton X-100 (Carl Roth, Germany). Primary antibodies were incubated overnight at 4 °C: anti-aggrecan (13880-1-AP, RRID: AB_2722780, 1:300; Proteintech) combined with anti-parvalbumin (PV235, RRID: AB_3698492, mouse IgG, 1:300; Swant, Switzerland), anti-GAD (M018-3, clone 9A6, RRID: AB_591728, mouse IgG1κ, 1:1000; MBL, USA), anti-vimentin (sc-66002, clone 5G3F10, RRID:AB_1131285, mouse IgG1κ, 1:100; Santa Cruz Biotechnology, USA), anti-non-phosphorylated neurofilament H (SMI32, 801701, RRID: AB_2564642, mouse IgG1, 1:200; BioLegend, USA) or anti-phospho-S6 ribosomal protein (pS6; 62016, Ser235/236, RRID: AB_2799618, mouse IgG2b, 1:800; Cell Signaling Technology, USA). Secondary antibodies were Alexa Fluor 647 goat anti-mouse IgG (A21235, RRID: AB_2535804) and Alexa Fluor 488 goat anti-rabbit IgG (A11070, RRID: AB_2534114; both 1:250; Thermo Fisher Scientific). Sections were counterstained with DAPI (Sigma-Aldrich, USA) and mounted in Fluorescence Mounting Medium (Agilent Dako). For perisomatic inhibitory terminals, triple immunofluorescence combined SMI32 (1:200), aggrecan (1:300) and the vesicular GABA transporter (VGAT; clone Ch117G4, 131009, RRID: AB_2943610, chicken IgY, 1:300; Synaptic Systems, Germany), detected with Alexa Fluor 647 goat anti-mouse IgG, Alexa Fluor 488 goat anti-rabbit IgG and Alexa Fluor 555 goat anti-chicken IgY (A32932, RRID: AB_2762844; all 1:250; Thermo Fisher Scientific). Additional triple immunofluorescence staining combining SMI32, VGAT, and synaptotagmin-2 (SYT2; 21245-1-AP, RRID: AB_3085646, rabbit IgG, 1:200; Proteintech) was performed to further characterize perisomatic inhibitory terminals associated with dysmorphic neurons. Primary antibodies were detected using Alexa Fluor 647-conjugated goat-anti-mouse IgG, Alexa Fluor 555-conjugated goat-anti-chicken IgY, and Alexa Fluor 488-conjugated goat-anti-rabbit IgG (all 1:250; Thermo Fisher Scientific).

Quantitative histology

Slides were digitized with Hamamatsu NanoZoomer S360 (brightfield) and S60 (fluorescence) scanners (Hamamatsu, Japan) and analyzed in QuPath (version 0.7.0) [9]. PNN density was

determined on aggrecan-immunostained sections within annotated control, lesional and perilesional cortex (minimum 2 mm^2 per region). Aggrecan-positive PNNs surrounding neuronal somata, and neurons immunoreactive for PV, GAD, SMI32 or pS6, alone or enwrapped by a PNN, were counted manually with the point annotation tool on double-labelled sections. Densities were expressed per mm^2, and the cellular identity of PNN-bearing cells was expressed as the proportion of marker-positive cells among all PNN-positive cells in the region.

Quantification of perisomatic VGAT-positive puncta

High-resolution images were acquired on a BZ-X810 fluorescence microscope (Keyence, Japan) with a 40x objective and identical acquisition settings for all specimens. In 11 FCDIIb specimens from eight patients, DN were classified as enwrapped (DN^{+PNN}) or not enwrapped by a PNN (DN^{-PNN}), and at least nine DN per group were randomly selected from lesional cortex of each specimen. In Fiji/ImageJ (version 2.16.0/1.54p) [70], the soma was delineated manually on the SMI32 channel. All subsequent steps were performed with a custom macro (Online Resource 2): conversion of the VGAT channel to 8-bit, binarization with the Default threshold algorithm, generation of a 3-µm perisomatic region of interest (ROI), and detection of VGAT-positive puncta with Analyze Particles (size 0.1–1.5 μm^2, circularity 0.2–1.0). Puncta counts were normalized to somatic perimeter and expressed per 100 µm (Suppl. Fig. 3, Online Resource 1).

Transmission electron microscopy

One FCDIIb specimen was fixed in paraformaldehyde, transferred to ITO fixative (2.5% paraformaldehyde, 2.5% glutaraldehyde, 0.1 M cacodylate buffer), post-fixed in 1% osmium tetroxide and embedded in Epon. Semithin sections (1 µm) stained with toluidine blue were used to identify regions containing DN. Ultrathin sections (50 nm; Ultracut, Leica, Germany) were contrasted with uranyl acetate and lead citrate, before examination with a Zeiss EM109 transmission electron microscope (Zeiss, Germany). DN were identified by an enlarged soma, abnormal cytoplasmic organization and accumulation of cytoskeletal filaments; synapses were classified as symmetric or asymmetric according to their pre- and postsynaptic membrane specializations.

Stereo-EEG recording and Chirp classification

Electrode trajectories were planned individually on the basis of electroclinical information and high-resolution 3D MRI. Implantations were performed under general anaesthesia with robot

guidance (Renishaw) using Spencer probe depth electrodes (Ad-Tech Medical Instrument Corporation, Racine, WI, USA); electrode explantation and resection were performed in a single session. SEEG was recorded with a Compumedics system (Compumedics, Australia) at a sampling rate of 500 Hz. For visual analysis, digital filter settings were adjusted as needed by the reviewer (high-pass 0.01–0.5 Hz, low-pass 70–250 Hz, 50 Hz notch). The spectral analysis was performed and reviewed with Persyst (Persyst Development Corporation, Solana Beach, CA, USA), with a maximum spectrogram frequency of 150 Hz. At least two seizures per patient were analyzed by computer-assisted time–frequency analysis [41]. Contacts with biomarker values above the upper limit of the 95% confidence interval across all channels were visually reviewed for low-voltage fast activity (LVFA) and Chirp patterns, defined as oscillatory activity with decreasing frequency over time. Contacts were classified, blinded to histology, as Chirp (clearly identifiable on the spectrogram with a corresponding oscillation in the SEEG trace), subtle Chirp (discernible only after frequency-specific normalization, without a clear correlate in the trace) or non-Chirp.

Co-registration and spatial analysis around electrode contacts

SEEG contacts, MRI and histological sections were co-registered as described previously [66]. Contacts segmented on the post-implantation CT were co-registered to the post-implantation 3D T_1-weighted MRI (3D Slicer version 5.11.0). Resected specimens were fixed in 4% buffered formalin, cut into 5-mm slabs perpendicular to the anterior–posterior axis and photographed; slab photographs were aligned to the resliced MRI using electrode trajectories, sulcal pattern and grey–white matter boundary as landmarks, and contact positions were transferred to the histological section, where the electrode track, identified by macrophage-rich tissue resorption, served as an independent landmark (Fig. 4). Around each track, a circular annotation corresponding to the electrode diameter (1100 µm) was placed, and concentric ROIs were generated at 500-µm intervals up to 2500 µm from its center (Figs. 5a, 6a). ROIs were restricted to intact tissue. Within each ROI, SMI32-positive DN, aggrecan-positive PNNs and DN^{+PNN} were counted, and PV^+ interneurons and PV^+ interneurons with a PNN (PV^{+PNN}) were counted on adjacent sections double-labelled for PV and aggrecan. All counts were performed blinded to the Chirp classification.

Statistical analysis

Analyses were performed in GraphPad Prism (version 11.0.0) and jamovi (version 2.7) with the GAMLj module (version 3.7.1). All tests were two-tailed with $\alpha = 0.05$. Paired lesional and

perilesional regions were compared with the Wilcoxon matched-pairs signed-rank test, and more than two groups with the Kruskal–Wallis test followed by Dunn's multiple comparisons test. Age dependence of PNN density was assessed by Spearman's rank correlation and simple linear regression, with comparison of slopes between cohorts. To account for multiple contacts per patient, mean DN^{+PNN} density per contact was analyzed with a linear mixed-effects model with SEEG class as fixed effect, patient as random intercept and mean total DN density as covariate; PV^{+PNN} density was analyzed analogously with total PV^{+} density as covariate. Mean total DN and PV^{+} densities per contact were analyzed in separate linear mixed-effects models with SEEG class as a fixed effect and a random intercept for patient, without additional covariates. The percentage of PNN-enwrapped DN/PV^{+} was calculated separately for each distance interval and averaged across intervals. These contact-level mean percentages were analyzed using a linear mixed-effects model with SEEG class as fixed effect and random intercept for patient. Within each model, pairwise comparisons between SEEG classes were adjusted for multiple testing using the *Holm* method. Degrees of freedom for *F*-tests were estimated using the Satterthwaite approximation. Model assumptions were assessed by inspection of residual and Q-Q plots. For VGAT puncta, the median density per patient and DN class was compared with the Wilcoxon matched-pairs signed-rank test. Data are presented as median with interquartile range (IQR) unless indicated otherwise. Sample size was determined by tissue availability; no *a priori* power calculation was performed.

Results

Cohort characteristics

The FCDIIb cohort (in total 22 patients) comprised frontal (and in one case frontoparietal) lesions from patients operated between infancy and the fourth decade of life, with a median duration of epilepsy until surgery of 8.5 years (range 0.5–28 years) and complete postoperative seizure freedom (Engel class 1A) in 17 patients. Seizures arose exclusively or partly from sleep in 15 patients, including seven of the ten patients investigated with SEEG (Table 1). *Post-mortem* control cortex was obtained from individuals of a comparable age range (1–39 years; Table 1).

Perineuronal nets accumulate in lesional FCDIIb cortex and increase with age

Aggrecan immunohistochemistry revealed dense, lattice-like PNNs around neuronal somata and proximal dendrites in all specimens (Fig. 1d). PNN density was significantly increased in

lesional cortex compared with perilesional (adjusted $P = 0.008$) and control cortex (adjusted $P < 0.0001$), whereas perilesional and control cortex did not differ (adjusted $P = 0.63$; Fig. 1b). The increase was consistent within individual specimens ($P = 0.0039$, $n = 9$ pairs; Fig. 1c). PNN density increased with age in both FCDIIb (Spearman $r = 0.78$, $P < 0.001$) and control cortex ($r = 0.65$, $P = 0.03$), but more steeply in FCDIIb (slopes 0.269 vs. 0.052, $P = 0.0135$), and was higher in FCDIIb across the entire age range (Fig. 1a).

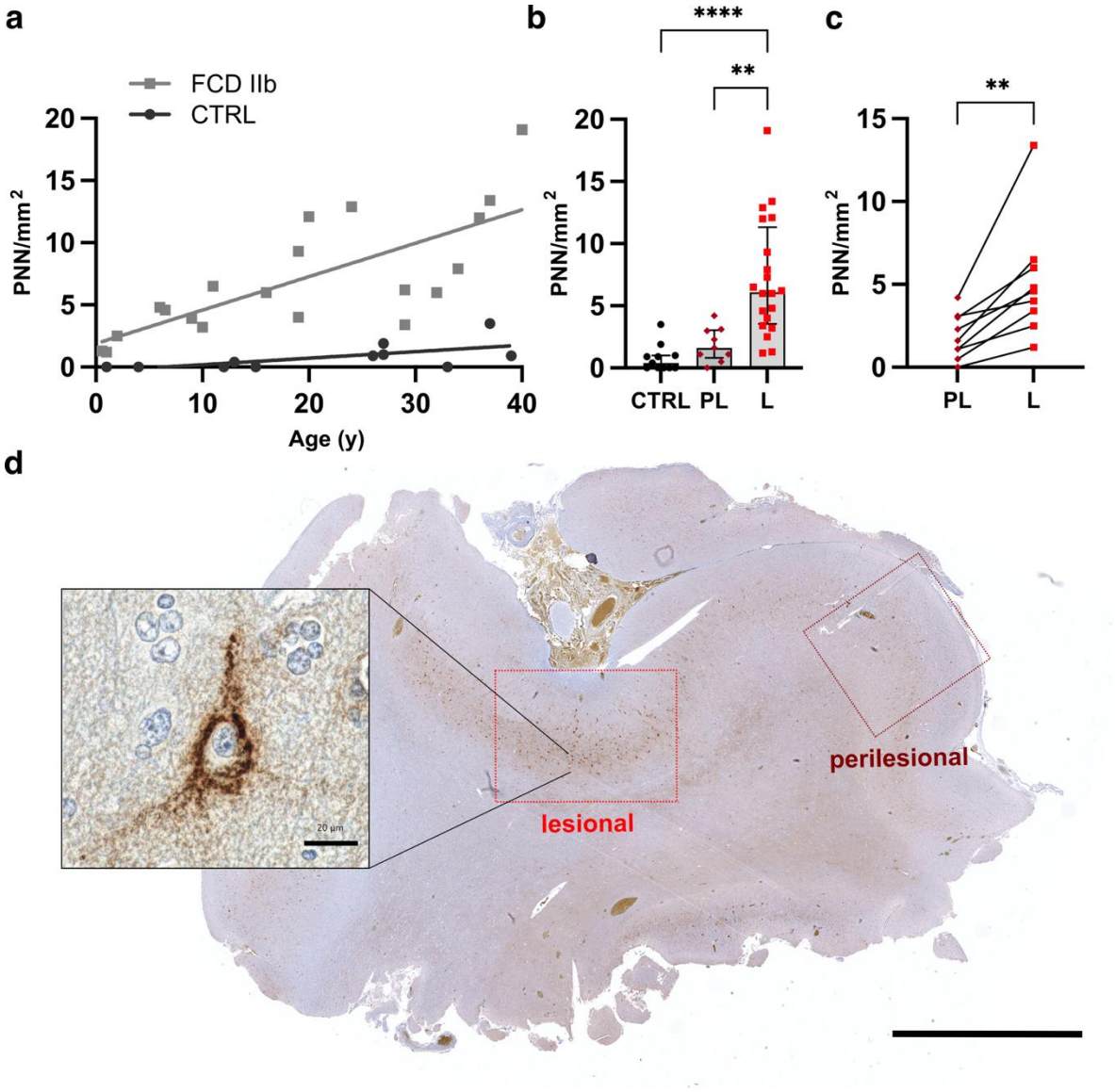


Fig. 1 Perineuronal nets accumulate in lesional FCDIIb cortex and increase with age. **a** PNN density (PNN/mm^2) correlates with age in FCDIIb (grey squares) and control cortex (CTRL, black circles), with consistently higher values in FCDIIb across the age range. **b** PNN density in control ($n = 11$), perilesional (PL, $n = 9$) and lesional FCDIIb cortex (L, $n = 20$). **c** Paired comparison of perilesional and lesional cortex within individual specimens; specimens without identifiable perilesional cortex were excluded. **d** Aggrecan immunohistochemistry of

a whole FCDIIb section with annotated lesional (bright red) and perilesional cortex (dark red). Scale bar 5 mm. *Inset*: aggrecan-positive PNN (brown, DAB) with haematoxylin counterstain. Scale bar 20 µm. Data are median with IQR. Statistics: Spearman correlation and linear regression (**a**), Kruskal–Wallis test with Dunn's correction (**b**), Wilcoxon matched-pairs signed-rank test (**c**). $^{**}P < 0.01$; $^{****}P < 0.0001$

Parvalbumin and GAD-positive interneurons are preserved but more frequently enwrapped by perineuronal nets

The density of PV^+ interneurons did not differ between control, perilesional and lesional cortex (control vs. perilesional, adjusted $P > 0.999$; control vs. lesional, adjusted $P > 0.999$; perilesional vs. lesional, adjusted $P > 0.999$; Fig. 2b; Table 2), nor did the density of GAD^+ neurons (control vs. perilesional, adjusted $P = 0.78$; control vs. lesional, adjusted $P > 0.999$; perilesional vs. lesional, adjusted $P = 0.26$; Table 2; Suppl. Fig. 1a, b, Online Resource 1). In contrast, PV^+ interneurons enwrapped by a PNN were increased in lesional cortex compared with perilesional (adjusted $P = 0.0187$) and control cortex (adjusted $P = 0.0010$; Fig. 2a, c), as were GAD^+ neurons with a PNN (adjusted $P = 0.0075$ and 0.0002; Suppl. Fig. 1c). Thus, PV^+ and other GABAergic interneurons are not lost in lesional FCDIIb cortex but acquire PNNs more frequently.

Perineuronal nets are recruited to dysmorphic neurons but not to balloon cells

The cellular allocation of PNNs differed markedly between regions (Table 2). In control cortex, 97% of PNN-bearing cells expressed PV and 83% GAD. In lesional cortex, these proportions fell to 52% and 60%, respectively, and perilesional cortex showed intermediate values (64% and 71%). Vimentin-positive balloon cells were never enwrapped by PNNs, neither in the grey nor in the white matter (Suppl. Fig. 2). Instead, a subset of DN, identified by strong SMI32 and pS6 immunoreactivity, carried aggrecan-positive PNNs that outlined their enlarged somata and proximal dendrites (Fig. 2d; Suppl. Fig. 1d). $SMI32^+$ and $pS6^+$ DN accounted for 27% and 24% of all PNN-bearing cells in lesional cortex, but only for 2% and 0.1% in perilesional cortex (Table 2). Both the density of DN and the density of DN^{+PNN} were markedly higher in lesional than in perilesional cortex ($P = 0.0039$ for $SMI32^+$ DN, $SMI32^+$ DN^{+PNN}, $pS6^+$ DN and $pS6^+$ DN^{+PNN}; Fig. 2e, f; Suppl. Fig. 1e, f). DN were absent from control cortex.

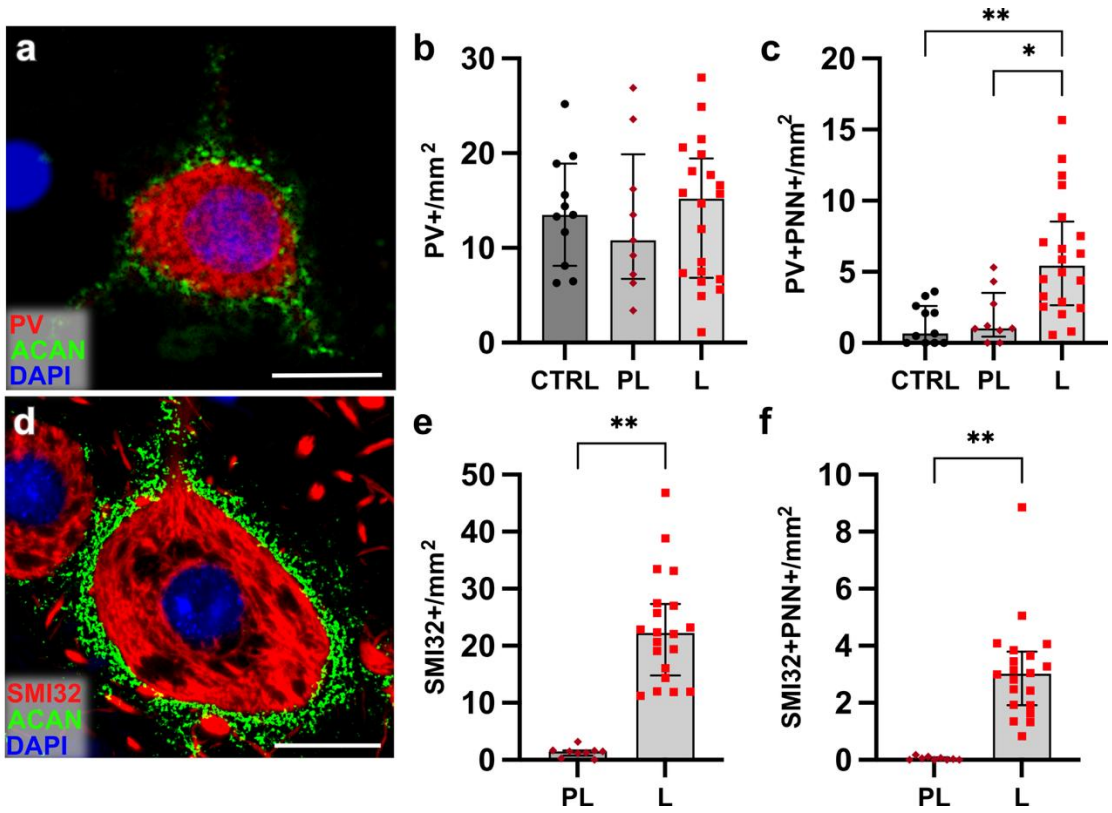


Fig. 2 Perineuronal nets are extended from parvalbumin interneurons to dysmorphic neurons in lesional FCDIIb cortex. **a** Aggrecan-positive PNN (ACAN, green) enwrapping a PV^+ interneuron (red); DAPI (blue). Scale bar 10 µm. **b** PV^+ cell density does not differ between control (CTRL, $n = 11$), perilesional (PL, $n = 9$) and lesional cortex (L, $n = 20$). **c** The density of PV^+ cells with PNN is increased in lesional cortex. **d** PNN (green) enwrapping an SMI32-positive dysmorphic neuron (red); DAPI (blue). Scale bar 20 µm. **e** Density of SMI32-positive DN and **f** of SMI32-positive DN with PNN in perilesional and lesional cortex. Data are median with IQR. Statistics: Kruskal–Wallis test with Dunn's correction (**b**, **c**); Wilcoxon matched-pairs signed-rank test (**e**, **f**). *$P < 0.05$; **$P < 0.01$

Perisomatic inhibitory innervation is increased on perineuronal net-enwrapped dysmorphic neurons

VGAT-positive puncta lined the somatic membrane of DN and, in DN^{+PNN}, were frequently located within the meshes of the aggrecan-positive net (Fig. 3a, b), in the position known to be occupied by synaptic terminals and astrocytic processes in PNN-bearing neurons [13, 17]. Normalized to somatic perimeter, perisomatic VGAT-positive puncta density was higher in DN^{+PNN} than in DN^{-PNN}, both across individual neurons (Fig. 3d) and in the paired comparison of patient-level medians ($P = 0.0078$; $n = 8$ patients; Fig. 3e). This is consistent with the abnormal VGAT-positive perisomatic baskets recently described around DN in FCDII [28].

SYT2, a marker of PV^+ inhibitory boutons [76], partially colocalized with VGAT-positive puncta around DN (Suppl. Fig. 4), indicating that part of the perisomatic innervation originates from PV^+ interneurons. Ultrastructurally, DN identified on semithin sections by their enlarged somata and accumulation of cytoskeletal filaments received axosomatic synapses with symmetric pre- and postsynaptic membrane specializations, the ultrastructural signature of inhibitory synapses (Fig. 3c, f).

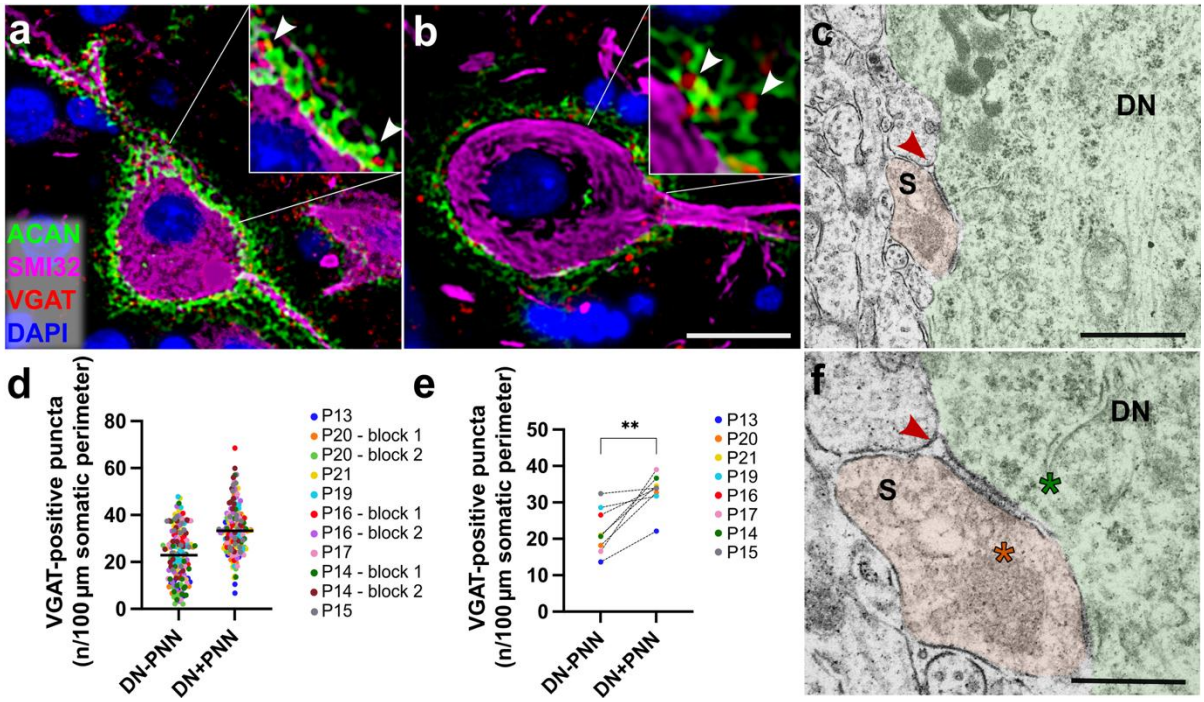


Fig. 3 Perisomatic inhibitory innervation is increased on dysmorphic neurons enwrapped by perineuronal nets. **a**, **b** Dysmorphic neurons with PNN (DN^{+PNN}) in FCDIIb tissue: SMI32 (magenta), aggrecan (ACAN, green), VGAT (red), DAPI (blue). *Insets* show VGAT-positive puncta along the somatic membrane and within the meshes of the PNN (white arrowheads). Scale bars 20 µm. **c** Electron micrograph of a DN (green; identified on semithin sections, not shown) receiving a symmetric synaptic contact (presynaptic terminal, orange); the synaptic cleft is marked by a red arrowhead. **d** Perisomatic VGAT-positive puncta per 100 µm somatic perimeter in individual DN without (DN^{-PNN}) and with PNN (DN^{+PNN}); colors distinguish individual tissue blocks, labeled by patient ID and block number where multiple blocks were analyzed from same patient, lines the overall median within each DN class. **e** Patient-level comparison; each point is the median of all DN analyzed in one patient, and paired values from the same patient are connected. **f** Higher magnification of the synapse in **c** showing the presynaptic terminal (S, orange), the DN soma (green) and the synaptic cleft (red arrowhead).

Scale bars 500 nm (**c**) and 250 nm (**f**). n = 11 blocks of 8 patients, ≥9 DN per group and block. Statistics: two-tailed Wilcoxon matched-pairs signed-rank test (**e**). $^{**}P < 0.01$

Perineuronal net-enwrapped dysmorphic neurons are enriched around Chirp-generating stereo-EEG contacts

To relate these histopathological features to sites of seizure onset, we co-registered SEEG contacts, MRI and histological sections in the ten patients investigated with SEEG (Fig. 4). Sixteen contacts (six Chirp, four subtle Chirp and six non-Chirp) were localized within individual tissue sections and linked to their ictal SEEG signal (Fig. 4e). Around Chirp contacts, DN^{+PNN} densities were highest close to the trajectory and declined with distance, whereas subtle Chirp and non-Chirp contacts showed uniformly lower densities (Fig. 5a, b). No significant difference in total DN density was detected between pairwise comparisons of contact classes (non-Chirp vs. subtle Chirp: *Holm*-adjusted $P = 0.663$, subtle Chirp vs. Chirp: *Holm*-adjusted $P = 0.084$, non-Chirp vs. Chirp: *Holm*-adjusted $P = 0.084$; Fig. 5e). In a linear mixed-effects model adjusted for total DN density and patient, SEEG class remained associated with DN^{+PNN} density [$F(2, 6.83) = 13.89$, $P = 0.004$]; Chirp contacts showed a higher DN^{+PNN} density than non-Chirp contacts ($\beta = 1.74$ cells/mm^2, 95% confidence interval 1.00–2.47, $P < 0.001$; Fig. 5c), and total DN density was not independently associated with DN^{+PNN} density ($\beta = 0.049$, 95% confidence interval −0.020 to 0.118, $P = 0.137$). The mean percentage of PNN-enwrapped DN across distance intervals differed between contact classes [$F(2, 5.42) = 5.83$, $P = 0.045$; Fig. 5d]. Chirp contacts showed a higher proportion of DN enwrapped by a PNN than non-Chirp contacts ($\beta = 13.68$ percentage points, 95% confidence interval 4.84–22.50, $P = 0.014$). In contrast, PV^{+PNN} density was not associated with SEEG class after adjustment for total PV^+ density [$F(2, 12.0) = 1.67$, $P = 0.229$; Fig. 6a–c], and neither the proportion of PNN-enwrapped PV^+ cells [$F(2, 13) = 1.99$, $P = 0.176$; Fig. 6d], nor total PV^+ density differed significantly between contact classes [$F(2, 13) = 2.19$, $P = 0.151$; Fig. 6e].

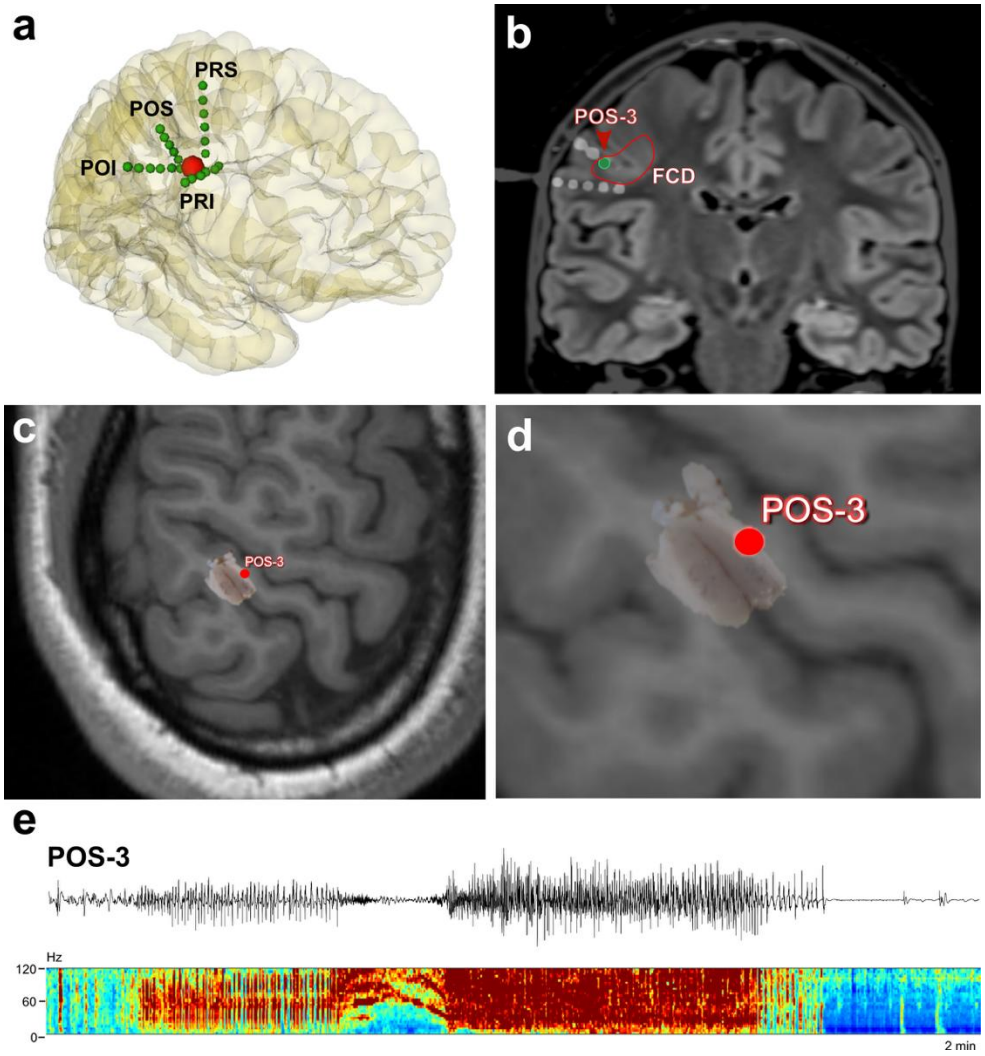


Fig. 4 Stereo-EEG–MRI–histology co-registration localizes Chirp-generating contacts in resected FCDIIb tissue. **a** Three-dimensional reconstruction of the cortical surface of patient P14 with the implanted SEEG electrodes (POI, POS, PRS, PRI; green contacts); the red sphere marks the region of convergence corresponding to the seizure onset zone. **b** Coronal FLAIR image showing the FCD (red outline) and the projected SEEG contacts; contact POS-3 (arrowhead) is located within the lesion. **c** Coronal T_1-weighted MRI with the resected specimen co-registered to its original anatomical position. **d** Same section as in **c**, with the location of contact POS-3 (red dot) projected onto the co-registered specimen. **e** SEEG recording from contact POS-3 during a habitual seizure (*top*) with the corresponding time–frequency spectrogram (*bottom*, 0–120 Hz): preictal spiking precedes the low-voltage fast-activity (LVFA) onset pattern, followed by evolution and postictal suppression. Time scale bar 2 min. FLAIR, fluid-attenuated inversion recovery

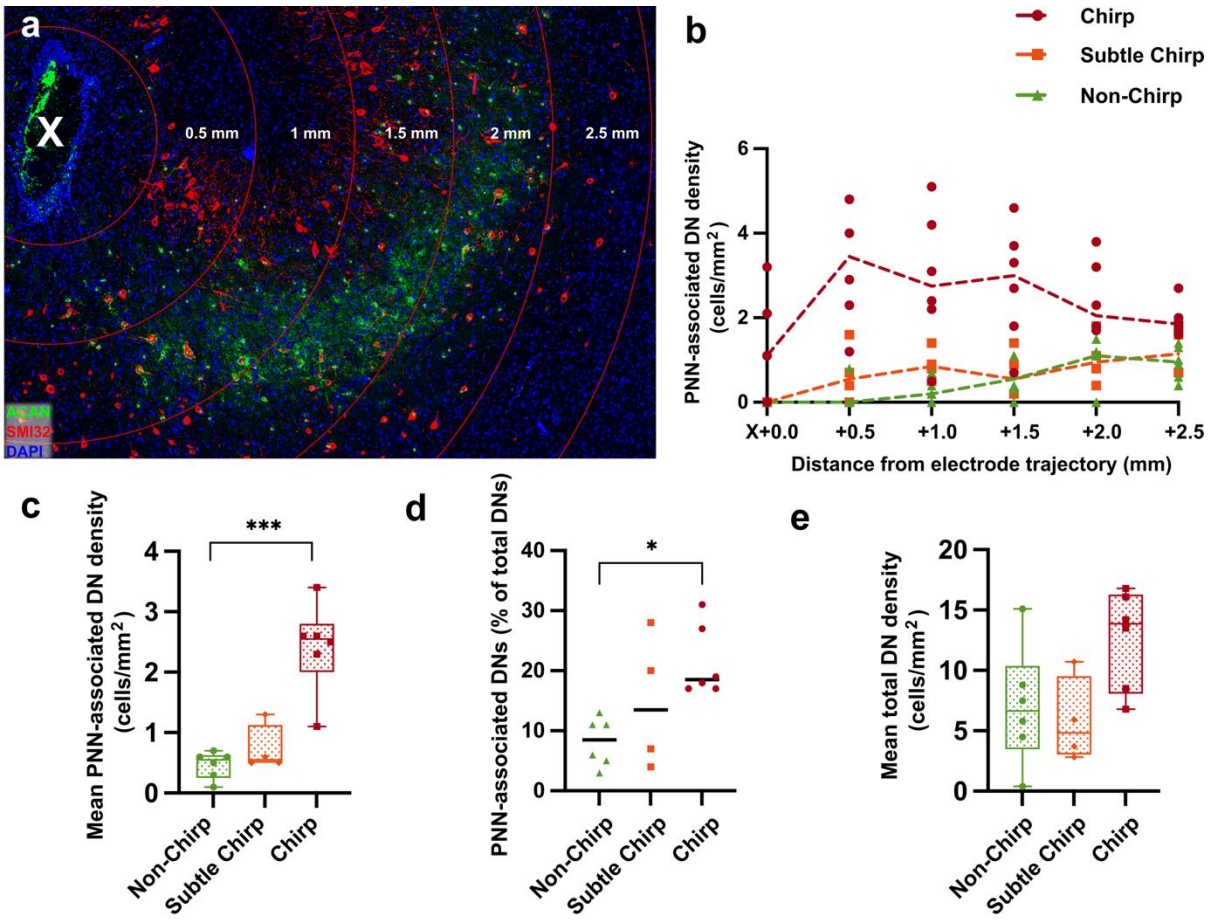


Fig. 5 Perineuronal net-enwrapped dysmorphic neurons are enriched around Chirp-generating stereo-EEG contacts. **a** Immunofluorescence of FCDIIb tissue for aggrecan (ACAN, green), SMI32 (red) and DAPI (blue). The histologically verified electrode trajectory (diameter 1.1 mm) is marked by X; concentric ROIs were placed at 0.5-mm intervals up to 2.5 mm from its centre. **b** Distance-dependent density of DN^{+PNN} around contacts classified as Chirp (red), subtle Chirp (orange) or non-Chirp (green); individual contacts are shown with the group median. **c** Mean DN^{+PNN} density per contact. **d** Proportion of DN enwrapped by a PNN among all DN per contact across distance intervals. **e** Mean total DN density per contact. Box plots show median, IQR and range. n = 6 Chirp, 4 subtle Chirp and 6 non-Chirp contacts from 10 patients. Statistics: linear mixed-effects model with SEEG class as fixed effect, patient as random intercept and total DN density as covariate (**c**); linear-mixed effects models with SEEG class as a fixed effect and a random intercept for patient (**d**, **e**). *$P < 0.05$; ***$P < 0.001$.

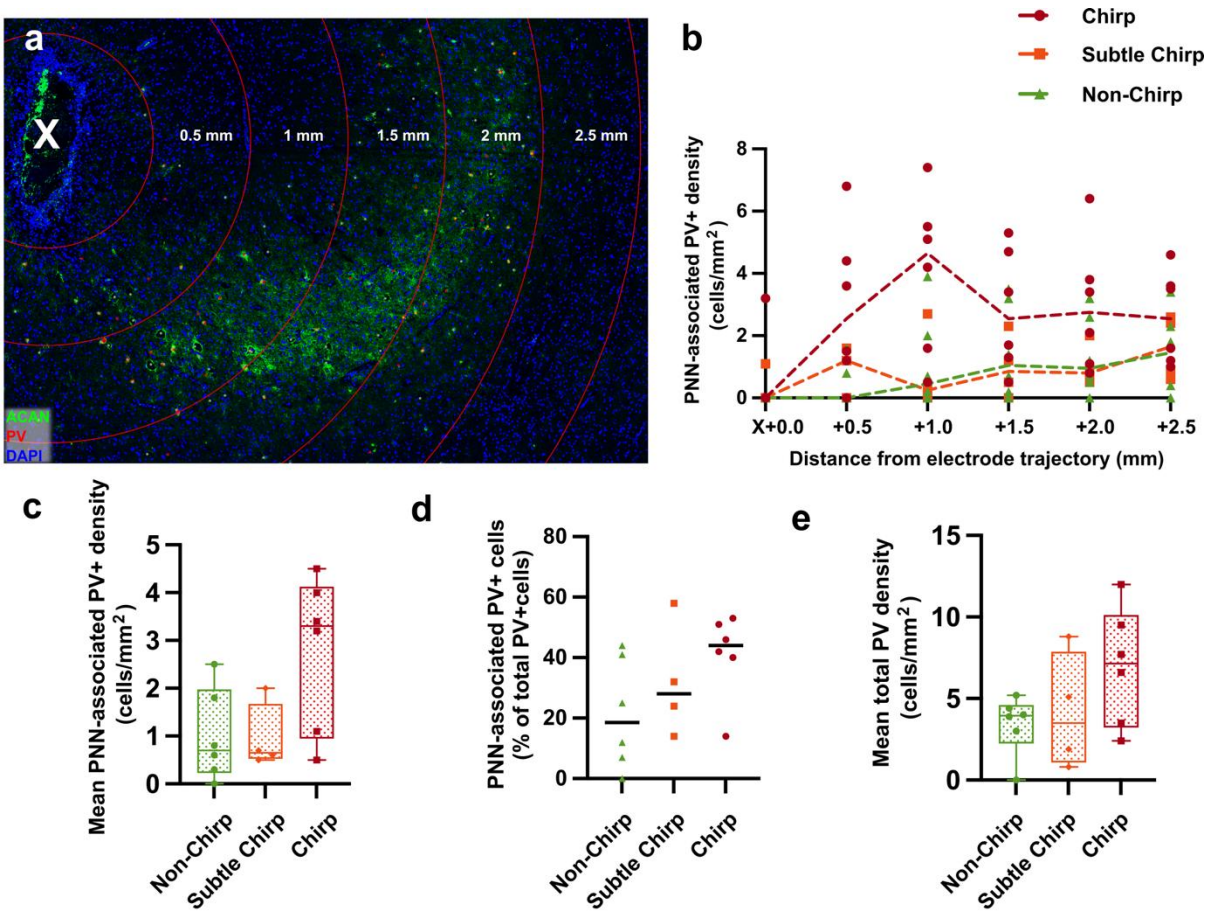


Fig. 6 Perineuronal net-enwrapped parvalbumin interneurons are not significantly altered around Chirp-generating stereo-EEG contacts. **a** Immunofluorescence of FCDIIb tissue for aggrecan (ACAN, green), parvalbumin (PV, red) and DAPI (blue); electrode trajectory (X) and concentric ROIs as in Fig. 5. **b** Distance-dependent density of PV^{+PNN} around Chirp (red), subtle Chirp (orange) and non-Chirp (green) contacts. **c** Mean PV^{+PNN} density per contact. **d** Proportion of PV^{+} interneurons enwrapped by a PNN. **e** Mean total PV^{+} density per contact. Box plots show median, IQR and range. n = 6 Chirp, 4 subtle Chirp and 6 non-Chirp contacts from 10 patients. Statistics: linear mixed-effects model with SEEG class as fixed effect, patient as random intercept and total PV^{+} density as covariate (**c**); linear-mixed effects models with SEEG class as a fixed effect and a random intercept for patient (**d**, **e**).

Discussion

This study provides a quantitative histopathological characterization of the perineuronal extracellular matrix in FCDIIb. We show that PNNs are increased in lesional cortex, that PV^{+} and other GABAergic interneurons are preserved but more frequently enwrapped by PNNs, and that PNNs are recruited to a subset of mTOR-activated DN, whereas balloon cells remain devoid of PNNs. PNN-enwrapped DN receive denser perisomatic GABAergic innervation,

partly from PV^+ terminals, and DN receive ultrastructurally verified symmetric synapses. Finally, PNN-enwrapped DN, independently of total DN density, are enriched around SEEG contacts generating the ictal-onset Chirp. Together, these findings define a lesion-specific microdomain of PNN-enwrapped PV^+ interneurons and DN within the dysplastic cortex.

Inhibitory interneurons and calcium-binding proteins in the human neocortex

Inhibition in the neocortex is provided by a heterogeneous population of GABAergic interneurons that account for about 20–25% of all neurons in primates [45] and differ in morphology, physiology, molecular profile and synaptic target domain [57, 83]. The CaBPs PV, calbindin-D28k and calretinin belong to the EF-hand family of Ca^{2+}-binding proteins and have long served as selective and complementary markers for these populations, both in the normal brain and in neuropathological conditions [2, 23, 29, 47]. In the primate and human neocortex, PV is expressed by fast-spiking basket and chandelier cells that innervate the soma, proximal dendrites and axon initial segment of pyramidal neurons; calbindin-D28k labels double-bouquet, Martinotti-type and neurogliaform cells, but also a subset of supragranular pyramidal neurons; and calretinin marks bipolar and double-bouquet cells, many of which preferentially innervate other interneurons [26, 29, 50]. Calretinin-positive interneurons are particularly abundant in the supragranular layers of the primate cortex [26, 47], and single-nucleus transcriptomics confirms that, despite a conserved basic architecture, human interneuron types differ from their rodent counterparts in proportions, laminar distribution and gene expression [46]. PV^+ interneurons represent a smaller fraction of neurons in human than in macaque visual cortex but include a higher proportion of large cells [14].

PV is a slow cytosolic Ca^{2+} buffer that shapes the time course of presynaptic Ca^{2+} transients and thereby short-term synaptic plasticity [19, 71], properties well suited to the high-frequency, temporally precise output of fast-spiking interneurons [48, 49]. Through powerful perisomatic synapses, PV^+ basket cells control spike timing of large pyramidal populations and generate network oscillations in the gamma range and above [10, 48]. This central position makes PV^+ interneurons a key element of both normal network function and epileptic synchronization, and reorganization of PV^+ basket and chandelier terminals is a recurrent finding in human epileptogenic cortex and hippocampus [3, 30, 56, 82].

Findings on interneurons in FCD have been divergent. Early immunocytochemical studies of Taylor-type dysplasia reported reduced numbers of CaBP-immunoreactive interneurons together with abnormal baskets of PV-positive terminals around giant neurons [38, 77], and

quantitative studies found reduced PV^+ cell densities in FCD type II [54, 88] or reduced GABAergic neuron densities [43, 87]. Abnormally large PV^+ and calbindin-positive local-circuit neurons have also been described within dysplastic foci [37]. In contrast, other studies found PV^+ and GAD-expressing neurons to be preserved in FCDII, with a redistribution rather than a loss of PV immunoreactivity [60], and an increased number of PV^+ perisomatic terminals on giant neurons in FCDIIb [80]. Our data favor the latter view: PV^+ and GAD^+ neuron densities were preserved in lesional cortex, and DN, particularly those enwrapped by PNNs, were densely innervated by VGAT- and partly SYT2-positive terminals. Garbelli et al. observed GABAergic terminals clustered around giant neurons without identifying synaptic contacts on their somata [38], whereas we and others [1, 72, 80] found symmetric axosomatic synapses on DN. Differences in the regions sampled (lesional vs. perilesional cortex), in the markers used and in the definition of DN may explain these discrepancies. Electrophysiological recordings from FCD tissue have shown reduced inhibitory postsynaptic current frequency and altered GABA uptake [20], indicating that preserved interneuron numbers do not necessarily imply preserved inhibitory function. Altered PV^+ circuitry in FCDIIb may therefore be better described as a local reorganization and reinforcement of fast perisomatic inhibition onto pathological principal cells than as a simple loss of inhibition. Whether calbindin- and calretinin-positive interneurons, which were not examined here, participate in this reorganization or are selectively affected remains to be determined.

Perineuronal nets under physiological and pathological conditions

PNNs are a specialized, highly organized form of extracellular matrix that enwraps the soma and proximal dendrites of particular neuronal populations, predominantly fast-spiking PV^+ interneurons in the neocortex [6, 24, 36]. They consist of hyaluronan anchored to the neuronal surface, chondroitin sulfate proteoglycans of the lectican family such as aggrecan and brevican, link proteins and tenascin-R [32, 36]. Their meshes are occupied by synaptic terminals and fine astrocytic processes, so that PNNs form a polyanionic microenvironment at the interface between neuron, synapse and astrocyte [13, 17, 81]. Several physiological functions have been attributed to this compartment: buffering of cations around highly active neurons and clustering of Kv3.1b channels [17, 44, 78], support of the fast-spiking phenotype and of PV^+ interneuron excitability [8, 35], restriction of synaptic plasticity at the closure of critical periods [21, 64], cooperation with astrocytes in potassium and transmitter uptake [81], and protection against oxidative stress and neurodegeneration [18, 61]. PNNs also shape the volume and geometry of the extracellular space [79].

In the human cortex, PNNs mature gradually during childhood and adolescence [58, 69], and their density continues to increase with age in the hippocampus, with a steeper rise in patients with temporal lobe epilepsy that has been interpreted as precocious ageing of the extracellular matrix [52]. Our observation of an age-dependent increase of neocortical PNN density that is steeper in FCDIIb than in control cortex extends this concept to a developmental malformation. Under pathological conditions, PNNs may be lost or reorganized. Reduced PNN densities have been reported in schizophrenia [58, 63], and in rodent models of acquired epilepsy, status epilepticus induces a persistent, activity-dependent degradation of PNN components [59, 67]. In human hippocampal sclerosis, PNNs are reduced in the sclerotic subfields [75], whereas PNN density is increased in the epileptic hippocampus as a whole [52], and PNN abnormalities have recently been described in different types of human epileptic tissue [28]. In that study, aggrecan immunoreactivity was altered in the core of FCDII lesions, and PNNs surrounded both PV^+ interneurons and DN bearing abnormal VGAT- and VGLUT1-positive perisomatic baskets [28]. FCDIIb thus represents a condition in which PNNs are not degraded but increased and extended to DN.

The recruitment of PNNs to DN is of particular interest. In healthy neocortex, PNNs around excitatory neurons are rare but exist, for example around a subpopulation of modified pyramidal cells in deep layers of the rat cortex [85]. DN are mTOR-activated principal cells with enlarged somata and an altered, partly immature molecular profile [4, 12]. The acquisition of an interneuron-like PNN phenotype by DN may reflect increased production of matrix components by these hypertrophic cells, an activity-dependent consolidation of their perisomatic synaptic input, or both. Because PNNs restrict structural plasticity [21, 64], their formation around DN may stabilize an abnormal synaptic configuration within the lesion. Balloon cells, which lack voltage-gated currents and synaptic input [25], never carried PNNs, supporting the view that PNN formation depends on neuronal activity and synaptic connectivity rather than on cell size or mTOR activation alone.

Implications for seizure onset

The spatial association between PNN-enwrapped DN and Chirp-generating contacts links these histopathological findings to the electrophysiology of seizure onset. LVFA at focal seizure onset is thought to be initiated by synchronized interneuronal activity rather than by principal cells [27, 33, 40, 74], and biophysical models reproduce this pattern through interneuron-driven accumulation of extracellular K^+ [39]. We therefore hypothesize that, within the PNN–PV–DN

microdomain, rhythmic PV$^+$ interneuron activity entrains densely innervated DN and generates the Chirp, and that a state-dependent failure of chloride and potassium homeostasis converts this local activity into a clinical seizure (Fig. 7). DN express altered chloride transporters, with increased NKCC1 and reduced or mislocalized KCC2 [4, 7, 43, 73], so that sustained GABAergic input may depolarize the GABA reversal potential [65]; experimentally, perisomatic inhibition becomes pro-ictal when chloride extrusion in the postsynaptic cell is insufficient [5, 55]. Factors associated with sleep and arousal, including BDNF–TrkB-dependent downregulation of KCC2 and changes in extracellular space volume, could provide the state dependence [68, 86] that explains the preferential occurrence of FCDII seizures from NREM sleep [34]. This model is derived from structural data and remains to be tested by direct recordings and chloride imaging in human tissue.

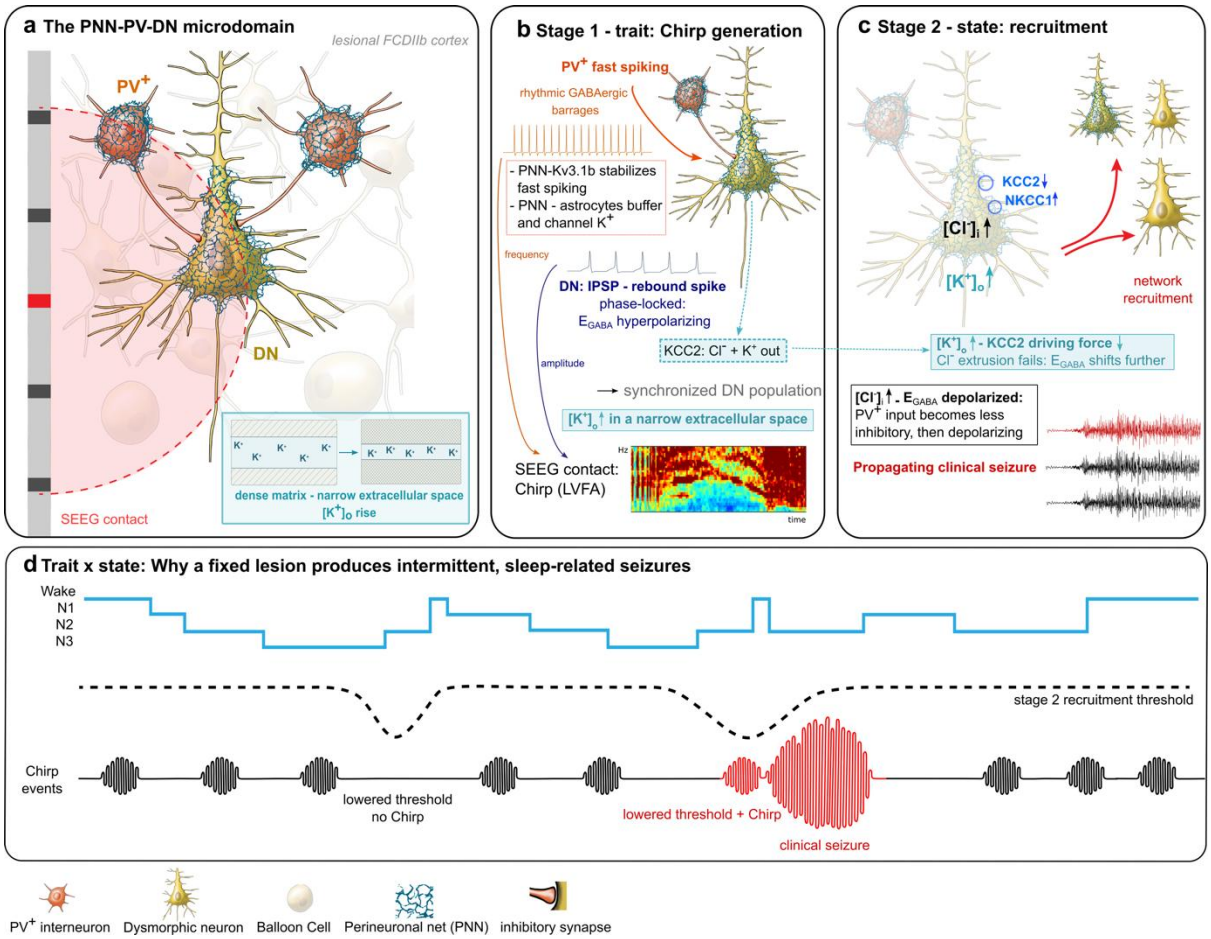


Fig. 7 Hypothetical model linking the PNN–PV–DN microdomain to seizure onset. **a** In lesional FCDIIb cortex, PV$^+$ basket cells, frequently enwrapped by PNNs, form perisomatic GABAergic synapses on PNN-enwrapped DN; balloon cells (BC) lack PNNs. The dashed circle indicates the approximate tissue volume sampled by a Chirp-generating SEEG contact; the blue box highlights the narrow interstitial compartment of the microdomain. **b** Stage 1

(trait): rhythmic PV^+ firing, supported by PNN-stabilized Kv3.1b channels, sets the frequency of the Chirp and entrains DN through perisomatic inhibition; KCC2-mediated Cl^- extrusion is coupled to K^+ efflux, so that K^+ accumulates in the narrow interstitial space (blue box). **c** Stage 2 (state): sustained activity and state-dependent factors of NREM sleep and arousal cause Cl^- accumulation in DN (NKCC1↑/KCC2↓), depolarize the GABA reversal potential (E_{GABA}) and convert local synchronization into recruitment of principal cells. **d** Trait × state gating: Chirps recur but remain local and subclinical while the recruitment threshold is high; a clinical seizure arises only when a Chirp coincides with a state-dependent lowering of the threshold, for example at NREM–arousal transitions. The model is a hypothesis derived from the present data and the literature; hypnogram and traces are schematic.

Limitations

This study has limitations. The cohort is modest and retrospective, no *a priori* power calculation was performed, and several contacts were derived from individual patients, which we addressed with mixed-effects models. Control tissue was obtained *postmortem*, which may influence antigen preservation. Limited sensitivity of the GAD antibody (clone 9A6) for somatic labeling may explain the lower GAD-positive than PV-positive fraction among PNN-enwrapped neurons in controls. Calbindin-D28k and calretinin were not examined, VGAT labels GABAergic terminals irrespective of interneuron subtype, and SYT2 colocalization was assessed qualitatively. Ultrastructural analysis was limited to one specimen, the analysis was two-dimensional, and co-registration error and tissue alterations along electrode tracks cannot be excluded.

Conclusions

In conclusion, FCDIIb is characterized by a lesion-specific increase of PNNs and their extension from PV^+ interneurons to DN, accompanied by preserved interneuron densities and reinforced perisomatic inhibitory innervation of PNN-enwrapped DN. The enrichment of these cells around Chirp-generating contacts identifies the perineuronal extracellular matrix as a structural correlate of the epileptogenic microcircuit in FCDIIb and as a potential target for future diagnostic and therapeutic approaches.

Declarations

Funding

This work was supported by the Deutsche Forschungsgemeinschaft (German Research Foundation), project 460333672, CRC1540 Exploring Brain Mechanics. The funder had no role in study design, data collection, analysis, interpretation or writing of the manuscript.

Competing interests

V.G. has advisory agreements with Brainlab AG and with Persyst Development Corporation, whose software was used for the SEEG analysis in this study; neither company had any role in the study design, data analysis, interpretation of the findings or the decision to publish. The other authors have no relevant financial or non-financial interests to disclose.

Ethics approval

This study was performed in line with the principles of the Declaration of Helsinki. The study was approved by the ethical review boards of the Medical Faculty of the Friedrich-Alexander University of Erlangen-Nuremberg (#193_18B, 18-192_1-Bio) and the University of Münster (2015-088-f-S).

Consent to participate

Written informed consent for the use of resected tissue for research purposes was obtained from all patients of their legal guardians.

Consent to publish

Not applicable; no identifying information about individual participants is included.

Data availability

The quantitative data underlying all graphs are available from the corresponding author upon reasonable request. Raw images and SEEG data are available upon reasonable request, subject to data protection regulations for patient data.

Code availability

The Fiji macro used to automate the VGAT puncta analysis is provided as Online Resource 2.

Use of AI-assisted tools

AI-assisted tools, including Claude (Anthropic) and ChatGPT (OpenAI), were used solely for language editing and improving readability. They were not used for study design, data

acquisition, data analysis, interpretation of findings or formulation of scientific conclusions. The authors critically reviewed all AI-assisted content and take full responsibility for the manuscript.

Author contributions

Conceptualization: Ingmar Blümcke; Methodology: Sophia Auer; Investigation: Sophia Auer, Johanna Samusch; Formal analysis and validation: Sophia Auer; Resources, software and data curation: Stefan Rampp, Vadym Gnatkovsky, Ahmed Gaballa, Lucas Hoffmann, Martin Schicht; Resources: Christian G. Bien, Till Hartlieb; Supervision: Friedrich Paulsen; Funding acquisition: Friedrich Paulsen, Ingmar Blümcke; Writing – original draft: Sophia Auer; Writing – review and editing: all authors. All authors read and approved the final manuscript.

References

1. Alonso-Nanclares L, Garbelli R, Sola RG, Pastor J, Tassi L, Spreafico R et al (2005) Microanatomy of the dysplastic neocortex from epileptic patients. Brain 128:158–173. https://doi.org/10.1093/brain/awh331
2. Andressen C, Blümcke I, Celio MR (1993) Calcium-binding proteins: selective markers of nerve cells. Cell Tissue Res 271:181–208. https://doi.org/10.1007/BF00318606
3. Arellano JI, Muñoz A, Ballesteros-Yáñez I, Sola RG, DeFelipe J (2004) Histopathology and reorganization of chandelier cells in the human epileptic sclerotic hippocampus. Brain 127:45–64. https://doi.org/10.1093/brain/awh004
4. Aronica E, Boer K, Redeker S, Spliet WG, van Rijen PC, Troost D et al (2007) Differential expression patterns of chloride transporters, Na+-K+-2Cl−-cotransporter and K+-Cl−-cotransporter, in epilepsy-associated malformations of cortical development. Neuroscience 145:185–196. https://doi.org/10.1016/j.neuroscience.2006.11.041
5. Assaf F, Schiller Y (2016) The antiepileptic and ictogenic effects of optogenetic neurostimulation of PV-expressing interneurons. J Neurophysiol 116:1694–1704. https://doi.org/10.1152/jn.00744.2015
6. Auer S, Schicht M, Hoffmann L, Budday S, Frischknecht R, Blümcke I et al (2025) The role of perineuronal nets in physiology and disease: insights from recent studies. Cells 14:321. https://doi.org/10.3390/cells14050321

7. Bakouh N, Castaño-Martín R, Metais A, Dan EL, Balducci E, Chhuon C et al (2025) Chloride deregulation and GABA depolarization in MTOR-related malformations of cortical development. Brain 148:549–563. https://doi.org/10.1093/brain/awae262

8. Balmer TS (2016) Perineuronal nets enhance the excitability of fast-spiking neurons. eNeuro 3:ENEURO.0112-16.2016. https://doi.org/10.1523/ENEURO.0112-16.2016

9. Bankhead P, Loughrey MB, Fernández JA, Dombrowski Y, McArt DG, Dunne PD et al (2017) QuPath: open source software for digital pathology image analysis. Sci Rep 7:16878. https://doi.org/10.1038/s41598-017-17204-5

10. Bartos M, Vida I, Jonas P (2007) Synaptic mechanisms of synchronized gamma oscillations in inhibitory interneuron networks. Nat Rev Neurosci 8:45–56. https://doi.org/10.1038/nrn2044

11. Blümcke I, Aronica E, Miyata H, Sarnat HB, Thom M, Roessler K et al (2016) International recommendation for a comprehensive neuropathologic workup of epilepsy surgery brain tissue: a consensus Task Force report from the ILAE Commission on Diagnostic Methods. Epilepsia 57:348–358. https://doi.org/10.1111/epi.13319

12. Blümcke I, Budday S, Poduri A, Lal D, Kobow K, Baulac S (2021) Neocortical development and epilepsy: insights from focal cortical dysplasia and brain tumours. Lancet Neurol 20:943–955. https://doi.org/10.1016/S1474-4422(21)00265-9

13. Blümcke I, Eggli P, Celio MR (1995) Relationship between astrocytic processes and “perineuronal nets” in rat neocortex. Glia 15:131–140. https://doi.org/10.1002/glia.440150205

14. Blümcke I, Hof PR, Morrison JH, Celio MR (1990) Distribution of parvalbumin immunoreactivity in the visual cortex of Old World monkeys and humans. J Comp Neurol 301:417–432. https://doi.org/10.1002/cne.903010307

15. Blümcke I, Spreafico R, Haaker G, Coras R, Kobow K, Bien CG et al (2017) Histopathological findings in brain tissue obtained during epilepsy surgery. N Engl J Med 377:1648–1656. https://doi.org/10.1056/NEJMoa1703784

16. Blümcke I, Thom M, Aronica E, Armstrong DD, Vinters HV, Palmini A et al (2011) The clinicopathologic spectrum of focal cortical dysplasias: a consensus classification proposed by an ad hoc Task Force of the ILAE Diagnostic Methods Commission. Epilepsia 52:158–174. https://doi.org/10.1111/j.1528-1167.2010.02777.x

17. Brückner G, Brauer K, Härtig W, Wolff JR, Rickmann MJ, Derouiche A et al (1993) Perineuronal nets provide a polyanionic, glia-associated form of microenvironment around certain neurons in many parts of the rat brain. Glia 8:183–200. https://doi.org/10.1002/glia.440080306

18. Cabungcal JH, Steullet P, Morishita H, Kraftsik R, Cuenod M, Hensch TK et al (2013) Perineuronal nets protect fast-spiking interneurons against oxidative stress. Proc Natl Acad Sci U S A 110:9130–9135. https://doi.org/10.1073/pnas.1300454110

19. Caillard O, Moreno H, Schwaller B, Llano I, Celio MR, Marty A (2000) Role of the calcium-binding protein parvalbumin in short-term synaptic plasticity. Proc Natl Acad Sci U S A 97:13372–13377. https://doi.org/10.1073/pnas.230362997

20. Calcagnotto ME, Paredes MF, Tihan T, Barbaro NM, Baraban SC (2005) Dysfunction of synaptic inhibition in epilepsy associated with focal cortical dysplasia. J Neurosci 25:9649–9657. https://doi.org/10.1523/JNEUROSCI.2687-05.2005

21. Carulli D, Pizzorusso T, Kwok JC, Putignano E, Poli A, Forostyak S et al (2010) Animals lacking link protein have attenuated perineuronal nets and persistent plasticity. Brain 133:2331–2347. https://doi.org/10.1093/brain/awq145

22. Celio MR (1986) Parvalbumin in most γ-aminobutyric acid-containing neurons of the rat cerebral cortex. Science 231:995–997. https://doi.org/10.1126/science.3945815

23. Celio MR (1990) Calbindin D-28k and parvalbumin in the rat nervous system. Neuroscience 35:375–475. https://doi.org/10.1016/0306-4522(90)90091-h

24. Celio MR, Blümcke I (1994) Perineuronal nets—a specialized form of extracellular matrix in the adult nervous system. Brain Res Brain Res Rev 19:128–145. https://doi.org/10.1016/0165-0173(94)90006-x

25. Cepeda C, André VM, Vinters HV, Levine MS, Mathern GW (2005) Are cytomegalic neurons and balloon cells generators of epileptic activity in pediatric cortical dysplasia? Epilepsia 46 Suppl 5:82–88. https://doi.org/10.1111/j.1528-1167.2005.01013.x

26. Condé F, Lund JS, Jacobowitz DM, Baimbridge KG, Lewis DA (1994) Local circuit neurons immunoreactive for calretinin, calbindin D-28k or parvalbumin in monkey prefrontal cortex: distribution and morphology. J Comp Neurol 341:95–116. https://doi.org/10.1002/cne.903410109

27. de Curtis M, Gnatkovsky V (2009) Reevaluating the mechanisms of focal ictogenesis: the role of low-voltage fast activity. Epilepsia 50:2514–2525. https://doi.org/10.1111/j.1528-1167.2009.02249.x

28. De Santis D, Cagnoli C, Biancheri D, Pastori C, Medici V, Calatozzolo C et al (2026) Perineuronal net abnormalities in epileptic human tissue. Epilepsia 67:5547–5559. https://doi.org/10.1002/epi.70368

29. DeFelipe J (1997) Types of neurons, synaptic connections and chemical characteristics of cells immunoreactive for calbindin-D28K, parvalbumin and calretinin in the neocortex. J Chem Neuroanat 14:1–19. https://doi.org/10.1016/s0891-0618(97)10013-8

30. DeFelipe J, Garcia Sola R, Marco P, del Río MR, Pulido P, Ramón y Cajal S (1993) Selective changes in the microorganization of the human epileptogenic neocortex revealed by parvalbumin immunoreactivity. Cereb Cortex 3:39–48. https://doi.org/10.1093/cercor/3.1.39

31. Di Giacomo R, Burini A, Chiarello D, Pelliccia V, Deleo F, Garbelli R et al (2024) Ictal fast activity chirps as markers of the epileptogenic zone. Epilepsia 65:e97–e103. https://doi.org/10.1111/epi.17995

32. Dityatev A, Schachner M (2003) Extracellular matrix molecules and synaptic plasticity. Nat Rev Neurosci 4:456–468. https://doi.org/10.1038/nrn1115

33. Elahian B, Lado NE, Mankin E, Vangala S, Misra A, Moxon K et al (2018) Low-voltage fast seizures in humans begin with increased interneuron firing. Ann Neurol 84:588–600. https://doi.org/10.1002/ana.25325

34. Eltze CM, Landre E, Soufflet C, Chassoux F (2020) Sleep related epilepsy in focal cortical dysplasia type 2: insights from sleep recordings in presurgical evaluation. Clin Neurophysiol 131:609–615. https://doi.org/10.1016/j.clinph.2019.11.055

35. Favuzzi E, Marques-Smith A, Deogracias R, Winterflood CM, Sánchez-Aguilera A, Mantoan L et al (2017) Activity-dependent gating of parvalbumin interneuron function by the perineuronal net protein brevican. Neuron 95:639–655.e10. https://doi.org/10.1016/j.neuron.2017.06.028

36. Fawcett JW, Oohashi T, Pizzorusso T (2019) The roles of perineuronal nets and the perinodal extracellular matrix in neuronal function. Nat Rev Neurosci 20:451–465. https://doi.org/10.1038/s41583-019-0196-3

37. Ferrer I, Pineda M, Tallada M, Oliver B, Russi A, Oller L et al (1992) Abnormal local-circuit neurons in epilepsia partialis continua associated with focal cortical dysplasia. Acta Neuropathol 83:647–652. https://doi.org/10.1007/BF00299415

38. Garbelli R, Munari C, De Biasi S, Vitellaro-Zuccarello L, Galli C, Bramerio M et al (1999) Taylor's cortical dysplasia: a confocal and ultrastructural immunohistochemical study. Brain Pathol 9:445–461. https://doi.org/10.1111/j.1750-3639.1999.tb00534.x

39. Gentiletti D, de Curtis M, Gnatkovsky V, Suffczynski P (2022) Focal seizures are organized by feedback between neural activity and ion concentration changes. eLife 11:e68541. https://doi.org/10.7554/eLife.68541

40. Gnatkovsky V, Librizzi L, Trombin F, de Curtis M (2008) Fast activity at seizure onset is mediated by inhibitory circuits in the entorhinal cortex in vitro. Ann Neurol 64:674–686. https://doi.org/10.1002/ana.21519

41. Gnatkovsky V, Pelliccia V, de Curtis M, Tassi L (2019) Two main focal seizure patterns revealed by intracerebral electroencephalographic biomarker analysis. Epilepsia 60:96–106. https://doi.org/10.1111/epi.14610

42. Grinenko O, Li J, Mosher JC, Wang IZ, Bulacio JC, Gonzalez-Martinez J et al (2018) A fingerprint of the epileptogenic zone in human epilepsies. Brain 141:117–131. https://doi.org/10.1093/brain/awx306

43. Han P, Welsh CT, Smith MT, Schmidt RE, Carroll SL (2019) Complex patterns of GABAergic neuronal deficiency and type 2 potassium-chloride cotransporter immaturity in human focal cortical dysplasia. J Neuropathol Exp Neurol 78:365–372. https://doi.org/10.1093/jnen/nlz009

44. Härtig W, Derouiche A, Welt K, Brauer K, Grosche J, Mäder M et al (1999) Cortical neurons immunoreactive for the potassium channel Kv3.1b subunit are predominantly surrounded by perineuronal nets presumed as a buffering system for cations. Brain Res 842:15–29. https://doi.org/10.1016/s0006-8993(99)01784-9

45. Hendry SH, Schwark HD, Jones EG, Yan J (1987) Numbers and proportions of GABA-immunoreactive neurons in different areas of monkey cerebral cortex. J Neurosci 7:1503–1519. https://doi.org/10.1523/JNEUROSCI.07-05-01503.1987

46. Hodge RD, Bakken TE, Miller JA, Smith KA, Barkan ER, Graybuck LT et al (2019) Conserved cell types with divergent features in human versus mouse cortex. Nature 573:61–68. https://doi.org/10.1038/s41586-019-1506-7

47. Hof PR, Glezer II, Condé F, Flagg RA, Rubin MB, Nimchinsky EA et al (1999) Cellular distribution of the calcium-binding proteins parvalbumin, calbindin, and calretinin in the neocortex of mammals: phylogenetic and developmental patterns. J Chem Neuroanat 16:77–116. https://doi.org/10.1016/s0891-0618(98)00065-9

48. Hu H, Gan J, Jonas P (2014) Fast-spiking, parvalbumin+ GABAergic interneurons: from cellular design to microcircuit function. Science 345:1255263. https://doi.org/10.1126/science.1255263

49. Kawaguchi Y, Katsumaru H, Kosaka T, Heizmann CW, Hama K (1987) Fast spiking cells in rat hippocampus (CA1 region) contain the calcium-binding protein parvalbumin. Brain Res 416:369–374. https://doi.org/10.1016/0006-8993(87)90921-8

50. Kawaguchi Y, Kubota Y (1997) GABAergic cell subtypes and their synaptic connections in rat frontal cortex. Cereb Cortex 7:476–486. https://doi.org/10.1093/cercor/7.6.476

51. Lamberink HJ, Otte WM, Blümcke I, Braun KPJ (2020) Seizure outcome and use of antiepileptic drugs after epilepsy surgery according to histopathological diagnosis: a retrospective multicentre cohort study. Lancet Neurol 19:748–757. https://doi.org/10.1016/S1474-4422(20)30220-9

52. Lehner A, Hoffmann L, Rampp S, Coras R, Paulsen F, Frischknecht R et al (2024) Age-dependent increase of perineuronal nets in the human hippocampus and precocious aging in epilepsy. Epilepsia Open 9:1372–1381. https://doi.org/10.1002/epi4.12963

53. Lévesque M, Gnatkovsky V, Li FR, Scalmani P, Uva L, Avoli M et al (2025) Fast activity chirp patterns in focal seizures from patients and animal models. Epilepsia 66:621–631. https://doi.org/10.1111/epi.18245

54. Liang C, Zhang CQ, Chen X, Wang LK, Yue J, An N et al (2020) Differential expression hallmarks of interneurons in different types of focal cortical dysplasia. J Mol Neurosci 70:796–805. https://doi.org/10.1007/s12031-020-01492-0

55. Magloire V, Cornford J, Lieb A, Kullmann DM, Pavlov I (2019) KCC2 overexpression prevents the paradoxical seizure-promoting action of somatic inhibition. Nat Commun 10:1225. https://doi.org/10.1038/s41467-019-08933-4

56. Marco P, Sola RG, Pulido P, Alijarde MT, Sánchez A, Ramón y Cajal S et al (1996) Inhibitory neurons in the human epileptogenic temporal neocortex. An

immunocytochemical study. Brain 119:1327–1347. https://doi.org/10.1093/brain/119.4.1327

57. Markram H, Toledo-Rodriguez M, Wang Y, Gupta A, Silberberg G, Wu C (2004) Interneurons of the neocortical inhibitory system. Nat Rev Neurosci 5:793–807. https://doi.org/10.1038/nrn1519

58. Mauney SA, Athanas KM, Pantazopoulos H, Shaskan N, Passeri E, Berretta S et al (2013) Developmental pattern of perineuronal nets in the human prefrontal cortex and their deficit in schizophrenia. Biol Psychiatry 74:427–435. https://doi.org/10.1016/j.biopsych.2013.05.007

59. McRae PA, Baranov E, Rogers SL, Porter BE (2012) Persistent decrease in multiple components of the perineuronal net following status epilepticus. Eur J Neurosci 36:3471–3482. https://doi.org/10.1111/j.1460-9568.2012.08268.x

60. Medici V, Rossini L, Deleo F, Tringali G, Tassi L, Cardinale F et al (2016) Different parvalbumin and GABA expression in human epileptogenic focal cortical dysplasia. Epilepsia 57:1109–1119. https://doi.org/10.1111/epi.13405

61. Morawski M, Brückner G, Jäger C, Seeger G, Arendt T (2010) Neurons associated with aggrecan-based perineuronal nets are protected against tau pathology in subcortical regions in Alzheimer's disease. Neuroscience 169:1347–1363. https://doi.org/10.1016/j.neuroscience.2010.05.022

62. Najm I, Lal D, Alonso Vanegas M, Cendes F, Lopes-Cendes I, Palmini A et al (2022) The ILAE consensus classification of focal cortical dysplasia: an update proposed by an ad hoc task force of the ILAE diagnostic methods commission. Epilepsia 63:1899–1919. https://doi.org/10.1111/epi.17301

63. Pantazopoulos H, Woo TU, Lim MP, Lange N, Berretta S (2010) Extracellular matrix-glial abnormalities in the amygdala and entorhinal cortex of subjects diagnosed with schizophrenia. Arch Gen Psychiatry 67:155–166. https://doi.org/10.1001/archgenpsychiatry.2009.196

64. Pizzorusso T, Medini P, Berardi N, Chierzi S, Fawcett JW, Maffei L (2002) Reactivation of ocular dominance plasticity in the adult visual cortex. Science 298:1248–1251. https://doi.org/10.1126/science.1072699

65. Raimondo JV, Burman RJ, Katz AA, Akerman CJ (2015) Ion dynamics during seizures. Front Cell Neurosci 9:419. https://doi.org/10.3389/fncel.2015.00419

66. Rampp S, Rössler K, Hamer H, Illek M, Buchfelder M, Doerfler A et al (2021) Dysmorphic neurons as cellular source for phase-amplitude coupling in focal cortical dysplasia type II. Clin Neurophysiol 132:782–792. https://doi.org/10.1016/j.clinph.2021.01.004

67. Rankin-Gee EK, McRae PA, Baranov E, Rogers S, Wandrey L, Porter BE (2015) Perineuronal net degradation in epilepsy. Epilepsia 56:1124–1133. https://doi.org/10.1111/epi.13026

68. Rivera C, Li H, Thomas-Crusells J, Lahtinen H, Viitanen T, Nanobashvili A et al (2002) BDNF-induced TrkB activation down-regulates the K+-Cl− cotransporter KCC2 and impairs neuronal Cl− extrusion. J Cell Biol 159:747–752. https://doi.org/10.1083/jcb.200209011

69. Rogers SL, Rankin-Gee E, Risbud RM, Porter BE, Marsh ED (2018) Normal development of the perineuronal net in humans; in patients with and without epilepsy. Neuroscience 384:350–360. https://doi.org/10.1016/j.neuroscience.2018.05.039

70. Schindelin J, Arganda-Carreras I, Frise E, Kaynig V, Longair M, Pietzsch T et al (2012) Fiji: an open-source platform for biological-image analysis. Nat Methods 9:676–682. https://doi.org/10.1038/nmeth.2019

71. Schwaller B (2020) Cytosolic Ca2+ buffers are inherently Ca2+ signal modulators. Cold Spring Harb Perspect Biol 12:a035543. https://doi.org/10.1101/cshperspect.a035543

72. Shao Y, Ge Q, Yang J, Wang M, Zhou Y, Guo JX et al (2022) Pathological networks involving dysmorphic neurons in type II focal cortical dysplasia. Neurosci Bull 38:1007–1024. https://doi.org/10.1007/s12264-022-00828-7

73. Shimizu-Okabe C, Tanaka M, Matsuda K, Mihara T, Okabe A, Sato K et al (2011) KCC2 was downregulated in small neurons localized in epileptogenic human focal cortical dysplasia. Epilepsy Res 93:177–184. https://doi.org/10.1016/j.eplepsyres.2010.12.008

74. Shiri Z, Manseau F, Lévesque M, Williams S, Avoli M (2016) Activation of specific neuronal networks leads to different seizure onset types. Ann Neurol 79:354–365. https://doi.org/10.1002/ana.24570

75. Sitaš B, Bobić-Rasonja M, Mrak G, Trnski S, Krbot Skorić M, Orešković D et al (2022) Reorganization of the brain extracellular matrix in hippocampal sclerosis. Int J Mol Sci 23:8197. https://doi.org/10.3390/ijms23158197

76. Sommeijer JP, Levelt CN (2012) Synaptotagmin-2 is a reliable marker for parvalbumin positive inhibitory boutons in the mouse visual cortex. PLoS One 7:e35323. https://doi.org/10.1371/journal.pone.0035323

77. Spreafico R, Battaglia G, Arcelli P, Andermann F, Dubeau F, Palmini A et al (1998) Cortical dysplasia: an immunocytochemical study of three patients. Neurology 50:27–36. https://doi.org/10.1212/wnl.50.1.27

78. Stevens SR, Longley CM, Ogawa Y, Teliska LH, Arumanayagam AS, Nair S et al (2021) Ankyrin-R regulates fast-spiking interneuron excitability through perineuronal nets and Kv3.1b K+ channels. eLife 10:e66491. https://doi.org/10.7554/eLife.66491

79. Syková E, Voříšek I, Starčuk Z, Kratochvíla J, Pavlova I, Ichikawa Y et al (2025) Disruption of extracellular matrix and perineuronal nets modulates extracellular space volume and geometry. J Neurosci 45:e0517242024. https://doi.org/10.1523/JNEUROSCI.0517-24.2024

80. Szekeres-Paraczky C, Szocsics P, Erőss L, Fabó D, Mód L, Maglóczky Z (2022) Reorganization of parvalbumin immunopositive perisomatic innervation of principal cells in focal cortical dysplasia type IIB in human epileptic patients. Int J Mol Sci 23:4746. https://doi.org/10.3390/ijms23094746

81. Tewari BP, Woo AM, Prim CE, Chaunsali L, Patel DC, Kimbrough IF et al (2024) Astrocytes require perineuronal nets to maintain synaptic homeostasis in mice. Nat Neurosci 27:1475–1488. https://doi.org/10.1038/s41593-024-01714-3

82. Tóth EZ, Szabó FG, Kandrács Á, Molnár NO, Nagy G, Bagó AG et al (2022) Perisomatic inhibition and its relation to epilepsy and to synchrony generation in the human neocortex. Int J Mol Sci 23:202. https://doi.org/10.3390/ijms23010202

83. Tremblay R, Lee S, Rudy B (2016) GABAergic interneurons in the neocortex: from cellular properties to circuits. Neuron 91:260–292. https://doi.org/10.1016/j.neuron.2016.06.033

84. Wang S, Li K, He Q, Yang H, Yang Y, Wang X et al (2025) Dysmorphic neurons with ultralow intrinsic excitability are paradoxically hyperexcitable in neural network in a

mouse model of focal cortical dysplasia type II. Epilepsia 66:4006–4022. https://doi.org/10.1111/epi.18498

85. Wegner F, Härtig W, Bringmann A, Grosche J, Wohlfarth K, Zuschratter W et al (2003) Diffuse perineuronal nets and modified pyramidal cells immunoreactive for glutamate and the GABA(A) receptor alpha1 subunit form a unique entity in rat cerebral cortex. Exp Neurol 184:705–714. https://doi.org/10.1016/S0014-4886(03)00313-3

86. Xie L, Kang H, Xu Q, Chen MJ, Liao Y, Thiyagarajan M et al (2013) Sleep drives metabolite clearance from the adult brain. Science 342:373–377. https://doi.org/10.1126/science.1241224

87. Yan L, Yun-Lin L, Yong-Ling L, Wei-Wei Z, Yue-Shan P (2023) Alteration of GABAergic neurons and abnormality of NKCC1/KCC2 in focal cortical dysplasia (FCD) type II lesions. Epilepsy Res 194:107180. https://doi.org/10.1016/j.eplepsyres.2023.107180

88. Zamecnik J, Krsek P, Druga R, Marusic P, Benes V, Tichy M et al (2006) Densities of parvalbumin-immunoreactive neurons in non-malformed hippocampal sclerosis-temporal neocortex and in cortical dysplasias. Brain Res Bull 68:474–481. https://doi.org/10.1016/j.brainresbull.2005.10.008

Table 1 Clinical characteristics of patients with FCDIIb and post-mortem controls and their inclusion in the individual analyses

ID	Sex	Loc.	Side	Age (y)	Onset (y)	Seizures	Dur. (y)	Engel	FU (mo)	IHC	SEEG (blocks)	VGAT (blocks)	TEM
P1	f	F	R	0.58	0.1	sleep/awake	0.5	1A	24	+	−	−	−
P2	m	F	R	1.8	0.5	sleep/awake	1	4A	182	+	−	−	−
P3	m	F	R	2.4	0.16	sleep/awake	2	1A	197	+	−	−	−
P4	f	F	L	6	0.25	awake	6	1A	254	+	−	−	−
P5	m	F	R	6.5	6	awake	0.5	1A	24	+	−	−	−
P6	f	F	L	10	3	sleep	7	1A	24	+	−	−	−
P7	f	F	R	13	5	awake	8	1A	6	+	−	−	−
P8	f	F	R	19	10	sleep	9	1A	24	+	−	−	−
P9	m	F	L	29	1	sleep	28	4B	166	+	−	−	−
P10	m	F	R	9.5	9	awake	0.5	1A	24	+	−	−	−
P11	f	F	R	32	4	sleep/awake	28	1C	72	+	−	−	−
P12	m	FP	L	5	2.25	sleep	3	1A	24	+	3	−	−
P13	f	F	R	15	6	awake	9	1A	24	+	1	1	−
P14	f	F	R	16	4	sleep	12	3A	26	+	2	2	−
P15	m	F	R	19	5	sleep	14	1A	6	+	1	1	−
P16	m	F	R	20	6	sleep	14	1A	24	+	2	2	−
P17	m	F	R	30	7	awake	23	1A	24	+	1	1	−
P18	m	F	L	31	4	sleep	27	1A	59	+	1	−	−
P19	f	F	L	36	12	awake	24	3A	6	+	1	1	−
P20	m	F	R	37	16	sleep	21	1A	24	+	3	2	−
P21	f	F	L	11	7	sleep	4	1A	24	−	1	1	−
P22	f	F	R	5.9	0.83	sleep	5	1A	23	−	−	−	+
CTRL1	m	F	–	1	n.a.	n.a.	n.a.	n.a.	n.a.	+	−	−	−
CTRL2	m	F	–	4	n.a.	n.a.	n.a.	n.a.	n.a.	+	−	−	−
CTRL3	f	F	–	12	n.a.	n.a.	n.a.	n.a.	n.a.	+	−	−	−
CTRL4	f	F	–	13	n.a.	n.a.	n.a.	n.a.	n.a.	+	−	−	−
CTRL5	m	F	–	15	n.a.	n.a.	n.a.	n.a.	n.a.	+	−	−	−
CTRL6	f	F	–	26	n.a.	n.a.	n.a.	n.a.	n.a.	+	−	−	−
CTRL7	f	F	–	27	n.a.	n.a.	n.a.	n.a.	n.a.	+	−	−	−
CTRL8	m	F	–	27	n.a.	n.a.	n.a.	n.a.	n.a.	+	−	−	−
CTRL9	m	F	–	33	n.a.	n.a.	n.a.	n.a.	n.a.	+	−	−	−
CTRL10	m	F	–	37	n.a.	n.a.	n.a.	n.a.	n.a.	+	−	−	−
CTRL11	f	F	–	39	n.a.	n.a.	n.a.	n.a.	n.a.	+	−	−	−

Age, age at surgery (patients) or at death (controls); Onset, age at seizure onset; Seizures, predominant occurrence of seizures from sleep, wakefulness or both; Duration, duration of epilepsy until surgery; Engel, postoperative seizure outcome according to Engel (1A, completely seizure-free since surgery; 1C, some disabling seizures after surgery but free of disabling seizures for at least 2 years; 3A, worthwhile seizure reduction; 4A, significant seizure reduction; 4B, no appreciable change); FU, postoperative follow-up. IHC, immunohistochemistry and immunofluorescence; SEEG, stereo-EEG–MRI–histology co-registration (number of tissue blocks with identifiable electrode trajectories); VGAT, quantification of perisomatic VGAT-positive puncta (number of tissue blocks); TEM, transmission electron microscopy. f, female; m, male; F, frontal; FP, frontoparietal; L, left; R, right; +, included; −, not included; n.a., not applicable.

Table 2 Cellular densities and identity of perineuronal net-bearing cells in control cortex and in perilesional and lesional FCDIIb cortex

	Control (n = 11)	FCDIIb perilesional (n = 9)	FCDIIb lesional (n = 20)
Cell density (cells/mm^2, mean ± SD)			
GAD$^+$ neurons	14.6 ± 6.1	17.2 ± 5.1	14.7 ± 6.5
PV$^+$ neurons	13.9 ± 5.8	13.0 ± 7.9	13.1 ± 7.3
SMI32$^+$ dysmorphic neurons	–	1.4 ± 0.9	23.2 ± 9.8
pS6$^+$ dysmorphic neurons	–	0.4 ± 0.4	19.8 ± 11.1
Identity of PNN-bearing cells (% of all PNN$^+$ cells)			
GAD$^+$	83	71	60
PV$^+$	97	64	52
SMI32$^+$	–	2	27
pS6$^+$	–	0.1	24

Cell densities were counted manually in areas of at least 2 mm^2 per region. Proportions are the mean percentages of marker-positive cells among all PNN-positive cells counted in the respective region; because the markers were analyzed on separate double-labelled sections, percentages do not add up to 100%. Dysmorphic neurons are absent from control cortex (–). GAD, glutamic acid decarboxylase; PV, parvalbumin; SMI32, non-phosphorylated neurofilament H; pS6, phospho-S6 ribosomal protein; PNN, perineuronal net

Supplementary Files

This is a list of supplementary files associated with this preprint. Click to download.

- OnlineResource2.pdf
- OnlineResource1.pdf